Available online at www.sciencedirect.com

SCIENCE DIRECT®

Thin Solid Films 480–481 (2005) 499–502

thin solid films

www.elsevier.com/locate/tsf

Properties of high-efficiency $CuInGaSe_2$ thin film solar cells

K. Ramanathan*, G. Teeter, J.C. Keane, R. Noufi

National Center for Photovoltaics, National Renewable Energy Laboratory, 1617 Cole Boulevard, Golden, CO 80401, United States

Available online 8 December 2004

Abstract

In this paper, we present recent results on the growth and characterization of $CuInGaSe_2$ (CIGS) thin film solar cells by the three-stage process. A conversion efficiency of 19.3% and 18.4% has been achieved for solar cells made from absorbers with band gap values of 1.15 and 1.21 eV, respectively. High open circuit voltages and fill factors are obtained. We attempt to relate these improvements to material and device properties. The results suggest that it might be possible to produce a 20% efficient solar cell by further optimization of the current collection.

Keywords: Efficiency; $CuInGaSe_2$; Solar cells

1. Introduction

Polycrystalline thin film solar cells based on CdTe and $CuInSe_2$ have been under rigorous development during the past decade. Both technologies are beginning to fulfill the promise of low-cost electric power generation from renewable energy sources. The technologies have matured to the point of commercial production, and their future looks bright. $CuInSe_2$ and its alloys with $CuGaSe_2$ and $CuInS_2$ have been studied for some time. There has been a steady increase in the efficiency of laboratory-scale devices, and the current best efficiencies are above 19% [1,2]. Production of large-area modules was pioneered by Shell Solar Industries [3], and vigorous efforts in Europe and Japan have added momentum to the goal of realizing 15% commercial size modules. Currently, the best module efficiencies are around 13% [4–6]. These accomplishments are even more remarkable when one compares the insufficient technological and science base of the CIS-based materials and that of Si photovoltaic technology. With the device technology maturing and the confidence in repeatability and yield increasing, more attention is given to the processes at the interfaces. Indeed, this ought to have been at the forefront because the properties of photovoltaic cells are dictated by the interactions that take place during the junction formation, and the electrical or electronic consequences of these interactions can be quite powerful. This knowledge is essential for tackling the next set of challenges. Some examples are: simplifying device structures to increase speed and throughput; fabricating high-efficiency solar cells without using CdS; and understanding the root cause of changes caused by voltage, humidity, and other perturbations. Differences exist between the processes used in the laboratories and in production, and this adds another dimension to the challenge of developing a comprehensive understanding of the issues. Nevertheless, useful lessons can be learned by judicious comparison of the properties of the various systems. The three-stage process represents one of the coevaporation methods for the fabrication of $CuInGaSe_2$ (CIGS) absorbers. The separation of the various stages allows careful control of film morphology and stoichiometry. The highest efficiency CIGS solar cells is fabricated by this process. In this paper, we report some of the properties of the absorbers and solar cells fabricated by the three-stage process.

2. Experimental

CIGS absorbers were grown on soda lime glass substrates with a sputter-deposited Mo layer [1]. The

* Corresponding author.
E-mail address: kannan_ramanathan@nrel.gov (K. Ramanathan).

0040-6090/$ - see front matter © 2004 Elsevier B.V. All rights reserved.
doi:10.1016/j.tsf.2004.11.050

absorber is grown by first depositing an $(InGa)_2Se_3$ layer and reacting it with Cu and Se. Compositional control was achieved by detecting the temperature change of the substrate during Cu-poor to Cu-rich transition at the end of the second stage. The third stage consists of the evaporation of In and Ga in the presence of Se. CdS deposition was performed using a solution consisting of 0.0015 M $CdSO_4$, 1.5 M NH_4OH, and 0.0075 M thiourea. The samples were immersed in the bath at room temperature and the temperature of the bath was increased to 60 °C. CdS thin films in the thickness range of 50–60 nm were deposited in 16 min. The ZnO layer was deposited in two stages. A 90-nm-thick undoped layer was first deposited from a pure ZnO target using Ar/O_2 working gas, and a second layer of about 120 nm was deposited from an Al_2O_3-doped ZnO target. The sheet resistance of the bilayer was about 65–70 Ω/□. Sputtering the undoped layer in oxygen ambient ensures high transmission and resistivity. Ni/Al grids were deposited by electron beam evaporation. The cell area was defined by photolithographic procedures and the cells were isolated by etching the ZnO and CdS layers. The total area of the cells was 0.408 cm^2. A 100-nm-thick MgF_2 film was deposited to serve as an antireflection coating. Current–voltage characteristics of the devices were measured under AM 1.5 Global spectrum for 1000 W/m^2 irradiance.

3. Results and discussion

We have fabricated a set of absorbers by varying the Ga content in the first stage of film growth while maintaining the Ga content of the third stage constant. This is a minor adjustment to our standard process specifications, and the experiment was designed to probe the effect of Ga content (in the bulk and surface regions) on the interface properties. Increasing the Ga/In flux ratio in the first stage increases the band gap of the absorbing region. In the following, we report the results from two growth runs. Samples S2212 and S2213 have an average Ga/(Ga+In) ratio of 0.26 and 0.31, respectively, as determined from electron microprobe analysis using an electron beam excitation energy of 10 kV. The average Cu/(In+Ga) ratios are in the range of 0.88–0.9. Fig. 1 shows a comparison of the scanning electron microscopy images of the two absorbers in plan view and cross section. The microstructure of S2212 (Fig. 1a and b) is similar to our previous samples with the same Ga content. S2213 has smaller grains near the substrate interface

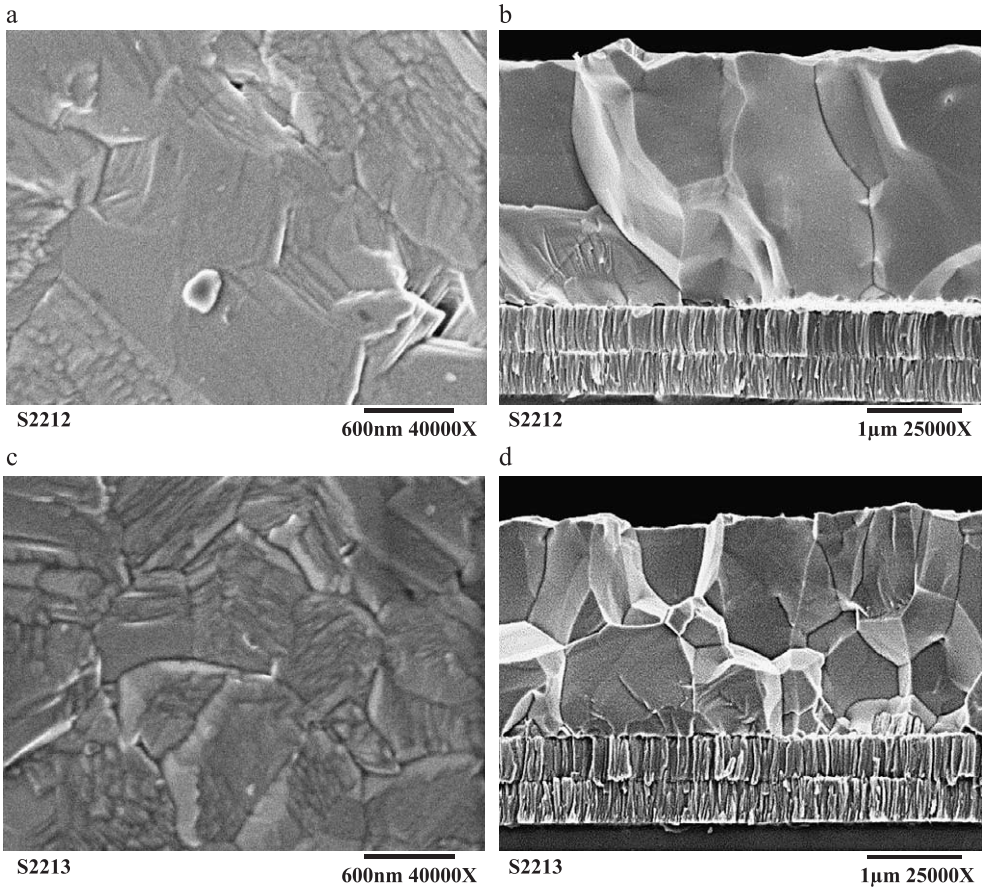

Fig. 1. Scanning electron microscope images of CIGS absorbers S2212 (a and b) and S2213 (c and d).

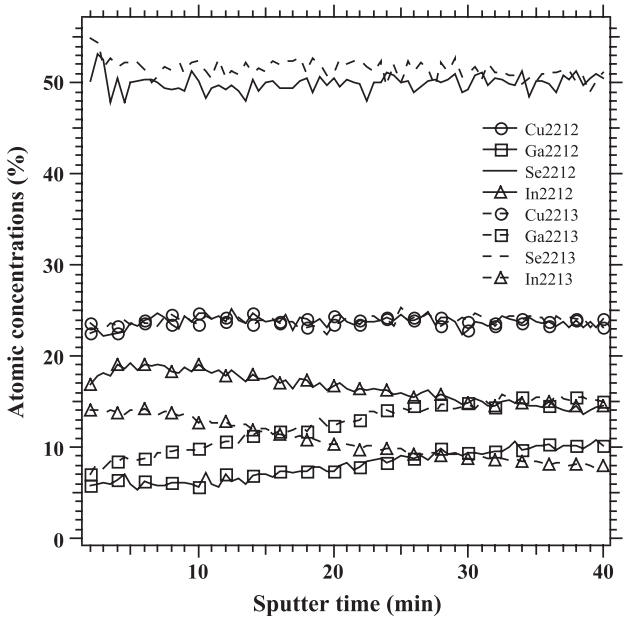

Fig. 2. Auger electron spectroscopy profiles of Cu, In, Ga, and Se as a function of sputter time for samples S2212 and S2213.

compared to S2212 (Fig. 1c and d). This is usually observed when the Ga content in the first stage is increased. The plan view images of both absorbers exhibit faceted grains typical of high-efficiency absorbers grown by the three-stage process. Fig. 2 shows the atomic concentrations of the various elements obtained by Auger depth profiling. We find that the increase of Ga in the first stage in sample S2213 has raised the Ga content in the bulk and surface regions. The profiles are also influenced by the diffusion kinetics of Ga. For example, the Ga profile of S2213 has a steeper slope, but the concentration near the surface is close to that of S2212. The average atomic concentrations obtained by electron microprobe measurements were used to derive the Auger sensitivity factors for Se and Cu. The Auger sensitivity factors for In and Ga were derived from electron microprobe measurements done on ungraded CIGS films.

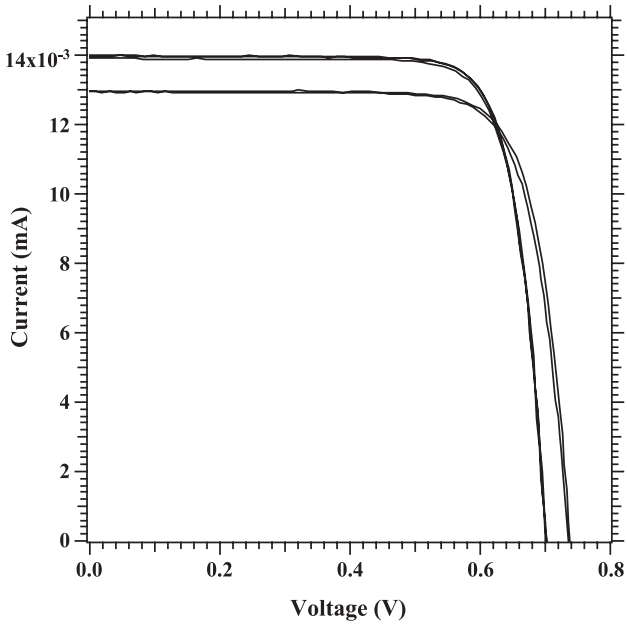

Fig. 3. Light *I–V* characteristics of solar cells from samples S2212 and S2213. Measured at 25 °C, AM 1.5 Global spectrum, 1000 W/m^2 irradiance. Total device area: 0.408 cm^2.

Table 1
Solar cell parameters for samples S2212 and S2213

Sample number	V_{oc} (V)	J_{sc} (mA/cm^2)	Fill factor (%)	Efficiency (%)
S2212-B1-3	0.701	34.60	79.65	19.3
S2212-B1-4	0.704	34.33	79.48	19.2
S2212-B1-5	0.703	34.08	79.23	19.0
S2213-A1-3	0.740	31.72	78.47	18.4
S2213-A1-4	0.737	31.66	78.08	18.2

Irradiance 1000 W/m^2, AM 1.5 Global spectrum, total device area 0.48 cm^2. Data provided by PV Performance Characterization Team, NREL.

Fig. 3 shows the current–voltage characteristics of three devices for sample S2212 and two devices for sample S2213. Open circuit voltages of 0.7 V and fill factors of nearly 80% are obtained for the sample with a nominal Ga/(In+Ga) ratio of 0.26. For the sample with an average Ga/(In+Ga) ratio of 0.31, the open circuit voltages are about 0.74 V. Fill factors are above 78%. The best conversion efficiencies for the two cases are 19.3% and 18.4%. The solar cell parameters are shown in Table 1. Dark and light current–voltage curves (*I–V*) for three cells from S2212 and two from S2213 were examined in detail. Table 2 shows the diode parameters extracted from analyzing the light current–voltage curves. The values determined from the dark *I–V* curves were similar. The series resistance was somewhat higher in the dark (~0.45 Ω.cm^2). The ideality factors (n) for S2212 cells are about 1.35, and for S2213, a value of ~1.6 was determined. The reverse saturation current density (J_0) under illumination is on the order of 10^{-11} A/cm^2 for the former and an order of magnitude higher for the sample with a higher band gap. Shunt resistances are high (10 kΩ cm^2) and series resistances are low (0.2–0.3 Ω cm^2) for all the devices. The high voltages and fill factors of all the cells can be related to the low ideality factors and reverse saturation current density, and, in turn, to the excellent quality of the CdS/CIGS interface.

Table 2
Diode parameters determined from light current–voltage curves

Device number	J_0 (A/cm^2)	n
S2212-B1-3	5×10^{-11}	1.35
S2212-B1-4	6×10^{-11}	1.36
S2212-B1-5	6×10^{-11}	1.35
S2213-A1-3	4×10^{-10}	1.57
S2213-B1-4	5×10^{-10}	1.62

J_0 is the reverse saturation current density, and n is the diode ideality factor.

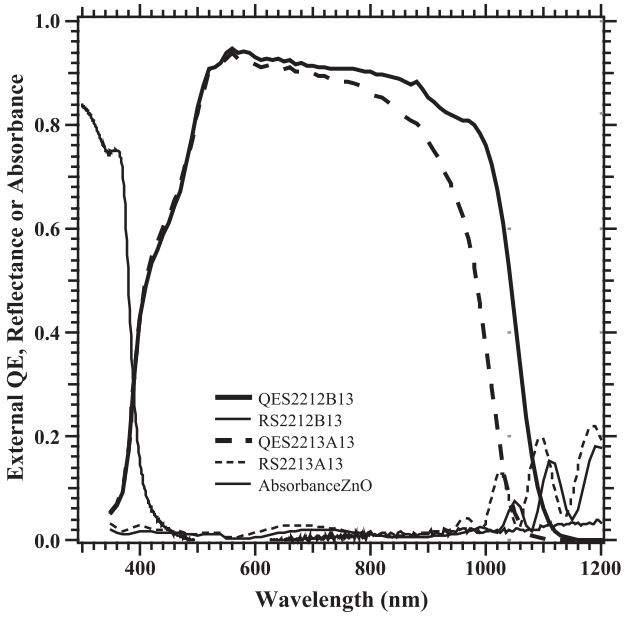

Fig. 4. External quantum efficiency and reflectance of solar cells. Absorbance of ZnO layer is also shown.

Fig. 4 shows the external quantum efficiency (QE) and reflectance of one cell from each sample. Also shown is the absorbance of the ZnO window layer, deduced from measurements of transmittance and reflectance of the film on borosilicate glass substrate. The reflectance and QE were measured simultaneously in the same apparatus. The MgF_2 antireflection coating is very effective in reducing the cell reflectance to negligible values. The optical loss in the ZnO layer is also minimal in the wavelength region of interest. The collection efficiency of both cells is above 90% in the visible spectral region. The decrease in the red region is partly due to the varying band gap and may not be a true collection loss. Band gap values were calculated by plotting the square of the spectral response vs. wavelength in the region of low collection. Energy gap values of 1.15 and 1.21 eV were calculated for samples S2212 and S2213. The short wavelength collection is reduced by absorption in the CdS window layer and the associated collection loss in the CdS layer or in the front part of the device. This presents an opportunity for improvement.

4. Conclusions

We have fabricated CIGS thin film solar cells with efficiencies at or above our previous record efficiency cells (19.0–19.3%). High efficiencies are also obtained for CIGS cells with a band gap of ~1.21 eV (18.4%). Analysis of the current–voltage curves shows that the high efficiency is related to low ideality factors and low reverse saturation current densities. The performance can be improved further by understanding the junction mechanisms and the collection losses in the short wavelength region.

Acknowledgments

This work was performed for the US DOE PV Program under contract no. DE-AC36-99GO10337 to NREL. The authors would like to thank M.A. Contreras, F.S. Hasoon, and B. Egaas for their help and support; B. To, A. Duda, J. Dolan, and J. Alleman for technical assistance; D. Dunlavy and T. Moriarty for cell characterization; and, L.L. Kazmerski for his encouragement. The authors are indebted to M. Gloeckler and J.R. Sites of the Colorado State University for their help in analyzing current–voltage curves.

References

[1] M.A. Contreras, B. Egaas, K. Ramanathan, J. Hiltner, A. Swartzlander, F. Hasoon, R. Noufi, Prog. Photovoltaics Res. Appl. 7 (1999) 311.
[2] K. Ramanathan, M.A. Contreras, C.L. Perkins, S. Asher, F.S. Hasoon, J. Keane, D. Young, M. Romero, W. Metzger, J. Ward, A. Duda, Prog. Photovoltaics Res. Appl. 11 (2003) 225.
[3] R.R. Gay, V. Probst, F.H. Karg, D.E. Tarrant, Proc. 3rd World Conf. Photovoltaic Energy Conversion, Osaka, Japan, May 11–18, 2003, p. 325.
[4] M. Powalla, B. Dimmler, Proc. 3rd World Conf. on Photovoltaic Energy Conversion, Osaka, Japan, May 11–18, 2003, p. 313.
[5] K. Kushiya, Proc. 3rd World Conf. Photovoltaic Energy Conversion, Osaka, Japan, May 11–18, 2003, p. 319.
[6] V. Probst, W. Stetter, J. Palm, R. Toelle, H.S. Visbeck, T. Calwer, H. Niesen, O. Vogt, M. Herenandez, F. Wendl, H. Karg, Proc. 3rd World Conf. Photovoltaic Energy Conversion, Osaka, Japan, May 11–18, 2003, p. 329.